NANOSYSTEMS:
PHYSICS, CHEMISTRY, MATHEMATICS

Original article

Jebisha S., et al. *Nanosystems: Phys. Chem. Math.*, 2024, **15** (6), 793–805.
http://nanojournal.ifmo.ru
DOI 10.17586/2220-8054-2024-15-6-793-805

$(CdO)_{1-x}(Mn_3O_4)_x$ ($x = 0.0/0.25/\ 0.50/0.75/1.0$) nanocrystals: preparation by a facile method, physicochemical properties and applications

Selvaraj Jebisha[1], Ganesan Deepa[2], Jesumarian Johnson[3], Chelliah K. Mahadevan[4]

[1]M.S. University, Tirunelveli, Tholayavattam-629167, Tamil Nadu, India
[2]Pioneer Kumaraswamy College, Nagercoil-629003, Tamil Nadu, India
[3]Annai Velankanni College, Tholayavattam-629167, Tamil Nadu, India
[4]Bharathidasan University, Tiruchirappalli-620024, Tamil Nadu, India

Corresponding author: G. Deepa, gdeepavinod@ymail.com; C. K. Mahadevan, mahadevan58@yahoo.co.in

ABSTRACT High phase pure $(CdO)_{1-x}(Mn_3O_4)_x$ ($x = 0.0/0.25/0.50/0.75/1.0$) nanocrystals (including multi-phased nanocomposites) were prepared by using a simple microwave-assisted solvothermal method, and characterized structurally, chemically, optically and electrically by carrying out X-ray diffraction, electron microscopic (SEM/TEM), energy dispersive X-ray absorption spectral, optical (UV-Vis) absorption spectral and AC electrical (at various temperatures and frequencies) measurements. Samples prepared exhibit crystalline nature, high chemical purity, nearly uniform spherical morphology, considerable particle sizes (within 47 nm), higher optical band gap energies (4.0 – 5.3 eV) and normal dielectric behavior. Studies were made to understand their capability in photocatalytic degradation (evaluated using Methylene Blue (MB) dye under UV-visible irradiation) and antimicrobial activity against gram positive Bacillus Subtilis (BS), gram negative Escherichia Coli (EC) and fungal Candida Albicans (CA). Results indicate a higher photocatalytic degradation with MB dye for the three multi-phased $(CdO)_{1-x}(Mn_3O_4)_x$ nanocomposites (with $x = 0.25/0.50/0.75$) prepared (with light of wavelength around 665 nm), and a higher antimicrobial activity with the bacteria (BS and EC) than with the fungus (CA); however, the phase pure Mn_3O_4 (with $x = 1.0$) nanocrystal has been found to be more active with all the three microbes considered.

KEYWORDS transition metal oxides nanocomposites, microwave-assisted solvothermal method, physicochemical properties, photocatalytic degradation, antimicrobial activity

ACKNOWLEDGEMENTS Authors are thanful to the Department of Physics and Research Centre of Annai Velankanni College, Tholayavattam, for providing AU 2603 UV-VIS Double Beam Spectrometer and Muffle furnace.

FOR CITATION Jebisha S., Deepa G., Johnson J., Mahadevan C.K. $(CdO)_{1-x}(Mn_3O_4)_x$ ($x = 0.0/0.25/0.50/0.75/1.0$) nanocrystals: preparation by a facile method, physicochemical properties and applications. *Nanosystems: Phys. Chem. Math.*, 2024, **15** (6), 793–805.

1. Introduction

Mn is a complex (but interesting) transition metal that may exist in a variety of oxidation states and can create a variety of oxides (including MnO, Mn_2O_3, Mn_3O_4 and MnO_2), which have a wide range of engineering applications. Cadmium oxide, crystallizing in a cubic rocksalt lattice (with anion centers and octahedral cation), due to its propensity to develop fault structures brought on by anion vacancies, it is uncommon in that it can be found in a variety of hues. The transition metal oxides (TMOs) such as cadmium oxide (CdO) and trimanganese tetraoxide (Mn_3O_4) have been found to be very interesting and highly useful in many applications when they are in nanocrystalline state. The CdO and Mn_3O_4 nanocrystals (nanoparticles) have been prepared in several ways with different morphologies; the crystallite (particle) size depends on the methods of preparation [1].

Nanocrystalline CdO (brown in color, an n-type semiconductor) has low electrical resistivity, high mobility and large refractive index, and has wide range of applications in cadmium plating baths, solar cells, electrodes for storage batteries, *etc*; also, it shows interesting photocatalytic degradation with methylene blue (MB) dye and antimicrobial activity [2–7]. There are several methods to prepare CdO nanoparticlessuch as solvothermal method, chemical method, hydrothermal method, sonochemical method, electrochemical method, microwave combustion method, thermal evaporation method, *etc.*; and they have been found to have excellent morphologies like nanocubes, nanoclusters, rhombus, nanowires, nanotubes and nanorods [1–7].

Somasundaram *et al.* [5] have recently reported the hydrothermal synthesis of cubic CdO nanocrystals with crystallite size of about 40 nm. Christuraj *et al.* [6] have reported the prepartion of pure and Mn doped CdO nanoparticles, calcined at 400 °C by co-precipitation method. Very recently, Alaa Munshi *et al.* [8] have reported their comparative investigation

of physicochemical properties of CdO nanoparticles synthesized utilizing urea-assisted auto-combustion and microwave combustion methods. They have found the phase and crystallite size of CdO nanoparticles modified, indicating the influence of heat treatment (at 350 °C) and synthesis procedure.

Nanocrystalline Mn_3O_4 (having higher potential than MnO) is a mixed oxide possessing high capacity, low toxicity, low current density and large surface area; and its spinel structure has Mn^{2+} and Mn^{3+} ions occupying the tetrahedral and octahedral sites respectively [9, 10]. Mn_3O_4 nanoparticles prepared by microwave assisted method have excellent performance as supercapacitors [11]. Atique Ullah *et al.* [12] have successfully synthesized Mn_3O_4 nanoparticles and studied the degradation of MB dye using it. Rafi Shaik *et al.* [13] have obtained the antimicrobial activity against cancer cells using Mn_3O_4 nanoparticles. Kalaiselvan *et al.* [14] have shown that the difference in particle sizes has considerable impact on toxicity, magnetic anisotropy constant and other cubic spinel structure properties, which are the main factors for biomedical applications. Tiny nanoparticles have peculiar physical and chemical properties than their bulk counterparts; and many emerging technologies (including solar energy conversion, optical devices, optical imaging and biomedical detection and therapy) need hybrid nanomaterials with improved optical and electronic properties [15]. Moreover, multi-phased nanocomposites reveal some interesting charactreistics than mono-phased nanomaterials; $CdCO_3$–Mn_3O_4 [15], ZnO/In_2O_3 [16], ZnO/CdO/CeO_2 [17] and Mn_3O_4/ZnO/Eu_2O_3 [18] are examples. Sundar *et al.* [19] have prepared the two-component $Zn_xCd_{1-x}O$ (with $x = 0.0/0.2/0.4/0.6/0.8/1.0$) nanocrystals by the microwave-assisted solvothermal technique (using a domestic microwave oven) and found that the optical bandgap energy changes from 2.24 – 3.06 eV when x is changed from 0.0 to 1.0; the phase purity occurred after annealing the as-prepared samples at 450 °C for 30 min. Nallendran *et al.* [20] have reported the photoconductive and photocatalytic properties of CdO–NiO nanocomposites synthesized by a cost-effective chemical method.

As nanocrystalline CdO and Mn_3O_4 are found to be very interesting, in order to discover new materials, an attempt has been made to prepare (by using the simple microwave-assisted solvothermal procedure, and easily available chemicals as precursors and solvent) and characterize (by determining their physicochemical properties using the available standard techniques) the two-component CdO-Mn_3O_4 (in different compositions) nanocrystals. As CdO and Mn_3O_4 are not isomorphous systems, it may not be possible for us to get lattice mixing sufficiently for the formation of mono-phased solid solutions with them. However, it is already known that creating a multi-component nanocomposite, whether it be mono or multi-phased, may result in the development of novel, intriguing features.

Earlier, Deepa and Mahadevan [21] have attempted to prepare the $(CdCO_3)_{0.5}(Mn_3O_4)_{0.5}$ nanocomposite (using cadmium acetate, manganese acetate and urea as the precursors, and ethylene glycol as the solvent) by a simple microwave-assisted solvothermal method using a domestic microwave oven; they found that the as-prepared sample (understood as $CdCO_3$–Mn_3O_4) has to be annealed at 300 °C to get the nanocomposite (two-phased) with higher phase purity, reduced crystallite size and homogeneity. Later, the same authors [15] have reported the synthesis and properties of un-doped and S^{2-} doped $(CdCO_3)_{1-x}(Mn_3O_4)_x$ nanocomposites (with $x = 0.0, 0.25, 0.50, 0.75$ and 1.0); the results of their thermal analysis have shown that when the as-prepared samples are annealed at more than 600 °C, two-phased nanocomposites (solid solutions) of $(CdO)_{1-x}(Mn_3O_4)_x$ (with $x = 0.0, 0.25, 0.50, 0.75$ and 1.0) can be prepared with high phase purity. So, in the present study, the $(CdO)_{1-x}(Mn_3O_4)_x$ (with $x = 0.0, 0.25, 0.50, 0.75$ and 1.0) nanocrystals (including multi-phased nanocomposites) were prepared by following the method adopted by Deepa and Mahadevan [15] along with annealing the prepared (As-prepared) samples at 650 °C, and then characterized structurally, chemically, optically and electrically. Moreover, photocatalytic degradation (evaluated using MB dye under UV-visible light irradiation) and antimicrobial activity (against gram positive Bacillus Subtilis, gram negative Escherichia Coli and fungus Candida Albicans) have been studied for the As-prepared (un-annealed) and annealed samples. The details are reported herein.

2. Experimental techniques

2.1. Materials

Analytical reagent (AR) grade precursors used in the present study arecadmium acetate dihydrate ($(CH_3COO)_2Cd{\cdot}2H_2O$), manganese acetate tetrahydrate ($(CH_3COO)_2Mn{\cdot}4H_2O$) and urea ($CH_4N_2O$); the solvent utilized was ethylene glycol. All the chemicals considered have beenused without any further purification.

2.2. Sample preparation

Method adopted by Deepa and Mahadevan [15] was used (along with annealing at 650 °C) to synthesise the proposed $(CdO)_{1-x}(Mn_3O_4)_x$ (with $x = 0.0, 0.25, 0.50, 0.75$ and 1.0) nanocrystals (a total of 5 samples). To create homogeneous solution, appropriate composition (x) of cadmium acetate dihydrate and manganese acetate tetrahydrate was dissolved in ethylene glycol (in a beaker); this solution was combined in a 1:3 molal ratio with urea and dissolved for 30 minutes with slight heating and strong stirring. The above solution (taken in a borosil bowl with lid) was microwave irradiated for about 15 – 20 min (till the formation of a colloidal precipitate) utilizing a domestic microwave oven (with 800 W power and 2.45 GHz frequency).

The resultant colloidal precipitate was cooled, washed with acetone three times, and then several times with double distilled water to eliminate any remaining organic contaminates, if any. This washed precipitate was filtered with whatman

filter paper and dried in open air atmosphere to get the As-prepared (un-annealed) sample. Finally, the five un-annealed samples obtained were annealed at 650 °C for 2 hin a muffle furnace to obtain the proposed (CdO)$_{1-x}$(Mn$_3$O$_4$)$_x$ (with $x = 0.0, 0.25, 0.50, 0.75$ and 1.0) nanocrystals. By using 2 ton hydraulic pressure, disk shaped pellets of 13 mm diameter (that were needed for some characterization investigations) were created from the powder samples.

The proposed powder samples prepared can be stored for a long time in self-locked covers. Fig. 1(a) shows a photograph of the five powder samples prepared [A1 ($x = 0.0$, CdO), A2 ($x = 0.25$, (CdO)$_{0.75}$(Mn$_3$O$_4$)$_{0.25}$), A3 ($x = 0.5$, (CdO)$_{0.5}$(Mn$_3$O$_4$)$_{0.5}$), A4 ($x = 0.75$, (CdO)$_{0.25}$(Mn$_3$O$_4$)$_{0.75}$) and A5 ($x = 1.0$, Mn$_3$O$_4$]. The As-prepared samples are represented here as U1, U2, U3, U4 and U5, respectively. The color of the As-prepared samples have been found to be intensified on annealing at 650 °C.

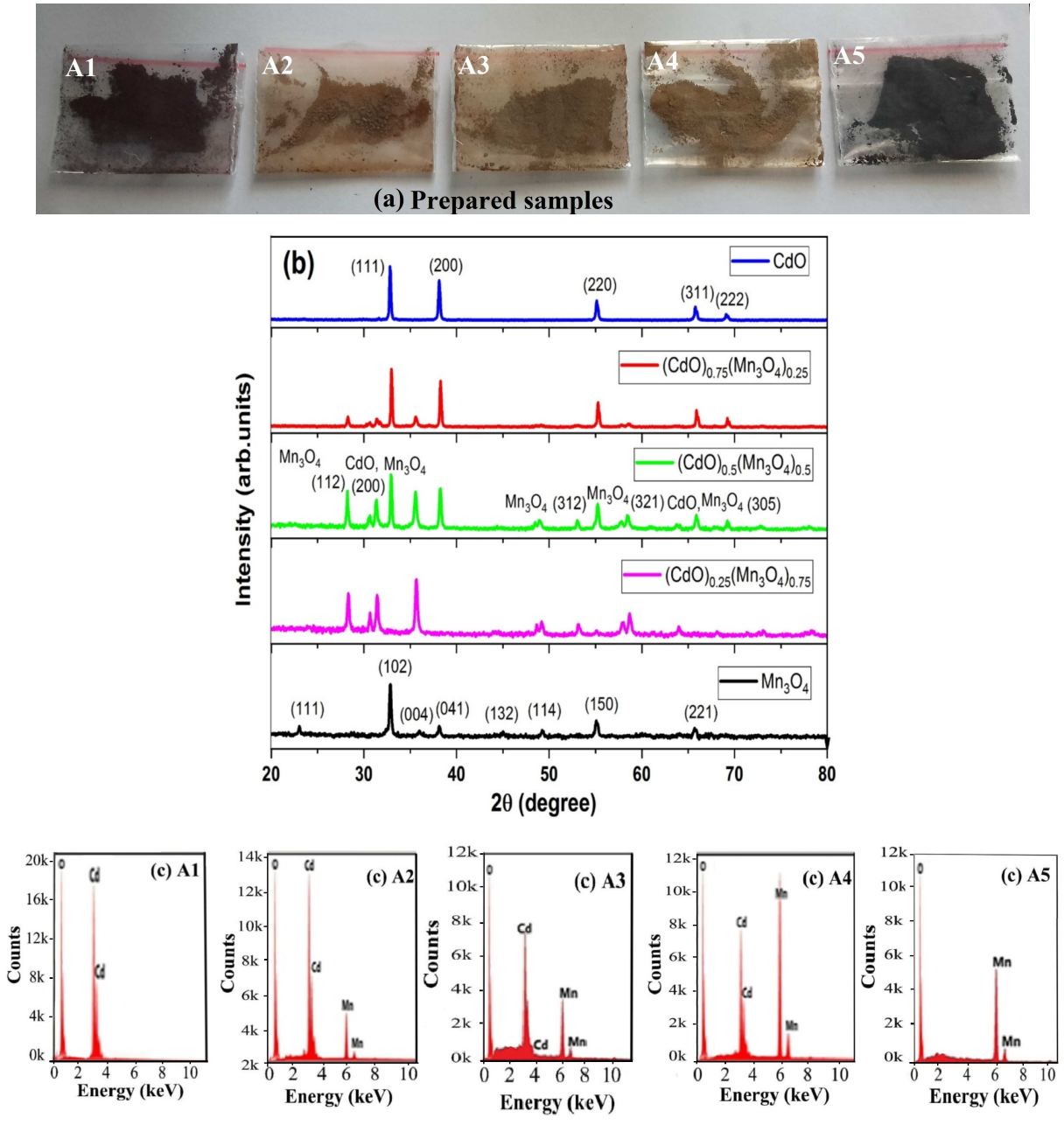

FIG. 1. A photograph showing the proposed powder samples prepared (a); The XRD patterns observed for the (CdO)$_{1-x}$(Mn$_3$O$_4$)$_x$ nanocrystals prepared (b); The EDX spectra observed for the (CdO)$_{1-x}$(Mn$_3$O$_4$)$_x$ nanocrystals prepared (c)

2.3. Characterization

All the five $(CdO)_{1-x}(Mn_3O_4)_x$ nanocrystals (A1, A2, A3, A4 and A5) prepared were characterized by determining their physicochemical properties using the available standard techniques. X-ray diffraction (XRD) patterns were made for all the five nanocrystals prepared using an XPERT-PRO X-ray diffractometer with monochromated CuKα (λ = 1.54060 Å) radiation in the 2θ range of 20 – 80°, with a scan speed of 2 °/min.

Scanning electron microscopic (SEM) images and energy dispersive X-ray absorption (EDX) spectra were recorded for all the five nanocrystals prepared using a JEOL SEM model, JSM5600LV scanning electron microscope with EDX attachment. Transmission electron microscopic (TEM) images were obtained for all the five nanocrystals prepared by using a JEOL 2011 transmission electron microscope, operating with a voltage of 200 kV; small area electron diffraction (SAED) pattern was also recorded for the sample A3.

The UV-V is (optical) absorption spectrum were captured in the wavelength range of 200 – 800 nm using a PerkinElmer UV-visible spectrophotometer (Lambda 35). The dielectric mesurements were carried out (within ± 2 % accuracy) by the parallel plate capacitor method [15] on pelletised samples using an LCR meter (Agilent 4284A) with five various applied field frequencies (100 Hz, 1 kHz, 10 kHz, 100 kHz and 1 MHz), and at twelve various temperatures between 40 – 150 °C (in step of 10 °C).

In order to understand the application potential of the samples prepared, evaluation of photocatalytic degradation (using MB dye under UV-visible light irradiation, with Xenon lamp) and antimicrobial activity against Bacillus Subtilis (+ive), Escherichia Coli (−ive) and Candida Albicans (fungal) was carried out for all the five annealed samples (CdO–Mn_3O_4). The study has been extended to three un-annealed samples ($CdCO_3$–Mn_3O_4 nanocomposites) also: U2 (x = 0.25, $(CdCO_3)_{0.75}(Mn_3O_4)_{0.25}$), U3 ($x = 0.5$, $(CdCO_3)_{0.5}(Mn_3O_4)_{0.5}$) and U4 ($x = 0.75$, $(CdCO_3)_{0.25}(Mn_3O_4)_{0.75}$).

3. Results and discussion

3.1. XRD analysis

Figure 1(b) displays the indexed XRD measurements observed for the $(CdO)_{1-x}(Mn_3O_4)_x$ nanocrystals (A1, A2, A3, A4 and A5) prepared. All the five patterns contain no peaks related to any impurity (other than peaks related to CdO and Mn_3O_4), which confirms the high phase purity of the samples prepared. Also, the sharp peaks are an indication of good crystallinity with reduced strain. The peaks observed for sample A1 at angles 32.84, 38.13, 55.11, 65.74 and 69.08° (corresponding to the crystal planes (111), (200), (220), (311) and (222), respectively) match well with the JCPDS card pattern for the CdO [JCPDS card No. 73-2245], and also with that reported earlier for CdO nanowires [22]. Also, the CdO nanocrystal is found to have the face centered cubic structure with space group $Fm\bar{3}m$, and the estimated lattice constant (a) is found to be 4.699 Å. The peaks observed for sample A5 at angles 23.05, 32.85, 38.13, 49.30, 55.03 and 65.73° (corresponding to the crystal planes (111), (102), (041), (114), (150) and (221), respectively) match well with the JCPDS card pattern for the Mn_3O_4 [JCPDS card No. 75-0765]. The Mn_3O_4 nanocrystal is found to have the orthorhombic structure with space group Pbcm, and the estimated lattice parameters are found to be: $a = 3.042$, $b = 9.682$ and $c = 9.571$ Å.

The PXRD patterns observed for the samples A2, A3 and A4 contain peaks corresponding to both CdO and Mn_3O_4 phases, which indicates that these samples are multi-phased $(CdO)_{1-x}(Mn_3O_4)_x$ nanocomposites. Changes observed in the XRD patterns for these nanocomposites with all of the end members (A1 and A5) indicate that mixing/alloying has taken place in them (A2, A3 and A4). However, few peaks appearingrelated to XRD of Mn_3O_4 in the middle composition match with that for the body-centered tetragonal phase of Mn_3O_4[JCPDS card No. 24-0734]; this is in agreement with that observed by Bousqet–Berthelin and Stuerga [23] for the Mn_3O_4 nanoparticles.

The average crystallite/particle size (D) values of the samples were estimated using the Scherrer's relation: $D = K\lambda/(\beta \cos\theta)$ [28], where λ refers wavelength of X-rays (= 1.54060 Å), θ is the Bragg angle of the major peak(s), $K = 0.9$ displays Scherrer's constant, and β is the full width (in radian) at half of maximum intensity of the major peak(s). The estimated D values are 45.2, 41.8, 40.4, 38.6 and 44.7 nm for the samples A1, A2, A3, A4 and A5, respectively. The D value is found to decrease with the increase in Mn concentration. However, for the Mn_3O_4, the value increases and becomes nearly equal to that for the CdO. Moreover, when compared with the un-annealed $[(CdCO_3)_{1-x}(Mn_3O_4)_x]$ nanocrystals (the D values vary from 6.6 to 21.0 nm, increasing as the Mn concentration increases) [15], the particle sizes of the annealed $[(CdO)_{1-x}(Mn_3O_4)_x]$ nanocrystals have increased more significantly along with improved crystallinity. However, the average crystallite sizes found in the present work compare well with that reported (40 nm) for the cubic CdO nanocrystals prepared by the hydrothermal method [5].

3.2. EDX spectral analysis

The observed EDX spectra for all the five $(CdO)_{1-x}(Mn_3O_4)_x$ nanocrystals prepared are shown in Fig. 1(c). The spectrum observed for CdO (A1) shows only Cd and O peaks and the spectrum observed for Mn_3O_4 (A5) shows only Mn and O peaks; and the spectra observed for the nanocomposites (A2, A3 and A4) show only Cd, Mn and O peaks. This shows the higher chemical purity of the nanocrystals prepared, and this result is in agreement with that observed through XRD analysis; also, formation of mixed nanocomposites is confirmed in the case of A2, A3 and A4 samples. It can be

seen that, for the mixed nanocomposites, the Cd content decreases nearly in proportion with the increase in x value; that is, the nanocomposites are properly formed as proposed.

3.3. SEM analysis

Figure 2(a) displays the SEM images obtained for all the five nanocrystals prepared; the SEM images reveal that most of the nanoparticles are agglomerated with spherical shape of different sizes. The end members (A1 and A5) are found to have regular and irregular spherical shapes. The nanocomposites (A2, A3 and A4) exhibit agglomerated spherical shape and cluster like patterns. In Fig. 2(a), it was observed that the average particle size from the SEM images varies between 40 – 65 nm [24, 25]. The average crystallite sizes observed from the XRD analysis for all the five nanocrystals prepared are found to be nearly two-third of the average particle sizes obtained through SEM analysis.

3.4. TEM and SAED analysis

The TEM imagesobtained for all the nanocrystals prepared (A1, A2, A3, A4 and A5), and the SAED pattern observed (as an illustration) for the sample A3 are shown respectively in Fig. 2(b,c). The TEM images indicate that the majority of particles appear to be agglomerated in spherical shape.The average particle sizes of the nanoparticles were found to be in the range from 50 – 90 nm [26, 27]. As with the SEM analysis, these are also found to be nearly two times of that obtained through XRD analysis. Furthermore, the TEM images observed have given similar results (regarding the shape of the particles) with that given by the SEM images observed. This shows that the average crystallite sizes obtained through XRD analysis (more valid for spherical and cubic shaped nanocrystals) can be considered as the average individual particle sizes.

The SAED pattern corresponding to the thin rings indicate the plane values such as (112), (211) and (325). The selected area electron diffraction (SAED) pattern observed for the sample A3 shows bright diffraction spots, which indicates a good crystallinity with polycrystalline aggregation [28]; the other samples can also be understood to have (in line with A3) better and good crystalline nature with polycrystalline aggregation.

3.5. UV-visible absorption spectral analysis

The UV-visible absorption spectra recorded in the present study are displayed in Fig. 3; the sharp and maximum absorption intensity peak (absorption band) appears in the UV region (within the wavelength range 230 – 310 nm) for all the five nanocrystals studied. Karthik *et al.* [2] have observed the absorption band for the CdO nanoparticle at around 225 nm. The intense absorption peaks observed in the UV region can be attributed mainly to the allowed charge transfer transitions, O^{2-} to Mn^{2+} and O^{2-} to Mn^{3+} [15]. The optical bandgap energy (E_g) values have been estimated from the absorption edges using the Planck's relation: $E_g = hc/\lambda$, where h specifies the Planck's constant, c refers velocity of light and λ refers wavelength of light (absorption edge). The E_g values obtained are 4.0 eV for A1, 4.7 eV for A2, 4.9 eV for A3, 5.3 eV for A4 and 4.6 eV for A5.

The E_g values observed are found to (nearly) depend on the average particle sizes of the samples; as the particle size increases the E_g value decreases [28]. The E_g value varies from 4.0 eV (for sample A1) to 5.3 eV (for sample A4); correspondingly, the D value varies from 45.26 nm (for sample A1) to 38.64 nm (for sample A4), which indicates that the absorption edge gets blue shifted. Morover, the E_g value increases with the rise in Mn content (x) in the case of nanocomposites (A2, A3 and A4) prepared. For the un-annealed samples [(CdCO$_3$)$_{1-x}$(Mn$_3$O$_4$)$_x$], particularly for the nanocomposites (with $x = 0.25$, 0.50 and 0.75), the spectra contain multiple absorption bands and E_g values [15]. It can be understood that the difference in optical absorption properties between the un-annealed [15] and annealed [present study] samples could be due to the differences in crystallinity, crystallite size, chemical difference, chemical phase purity, etc.

3.6. Dielectric properties

The dielectric measurements were performed on all the five pelletised samples prepared at twelve various temperatures and with five various frequencies by the parallel plate capacitor method. The dielectric constant (ε_r) and AC electrical conductivity (σ_{ac}) values were calculated from the measured capacitance (C) and dielectric loss factor ($\tan\delta$) values by using the relations: (1) $\varepsilon_r = (C/C_{\text{air}})$ and (2) $\sigma_{ac} = (\varepsilon_0)(\varepsilon_r)(\omega)(\tan\delta)$, where C_{air} is the air capacitance, (ε_0) is the permitivity of free space ($= 8.85 \cdot 10^{-12}$ C^{2}N^{-1}M^{-2}), ω refers the angular frequency ($= 2\pi f$), and f implies the frequency of the applied AC electric field.

The temperature dependences of dielectric constant, dielectric loss factor and AC electrical conductivity observed for all the five nanocrystals prepared are displayed in Fig. 4(a,b,c), respectively. The values ε_r and $\tan\delta$ values are observed to increase with increasing temperature, and fall with increasing frequency; the σ_{ac} value is found to increase with both temperature and frequency. This shows that all the five nanocrystals studied exhibit a normal dielectric behavior; however, sample A5 is found to have maximum dielectric constants among all the five samples considered.

The energy that a solid substance has accumulated from an applied AC electric field is known as the ε_r with increase of temperature can essentially be due to the temperature dependency of polarizability due to ionic, dipolar, electronic and space charge contributions; the higher ε_r values found at lower frequencies can be attributed to the space charge,

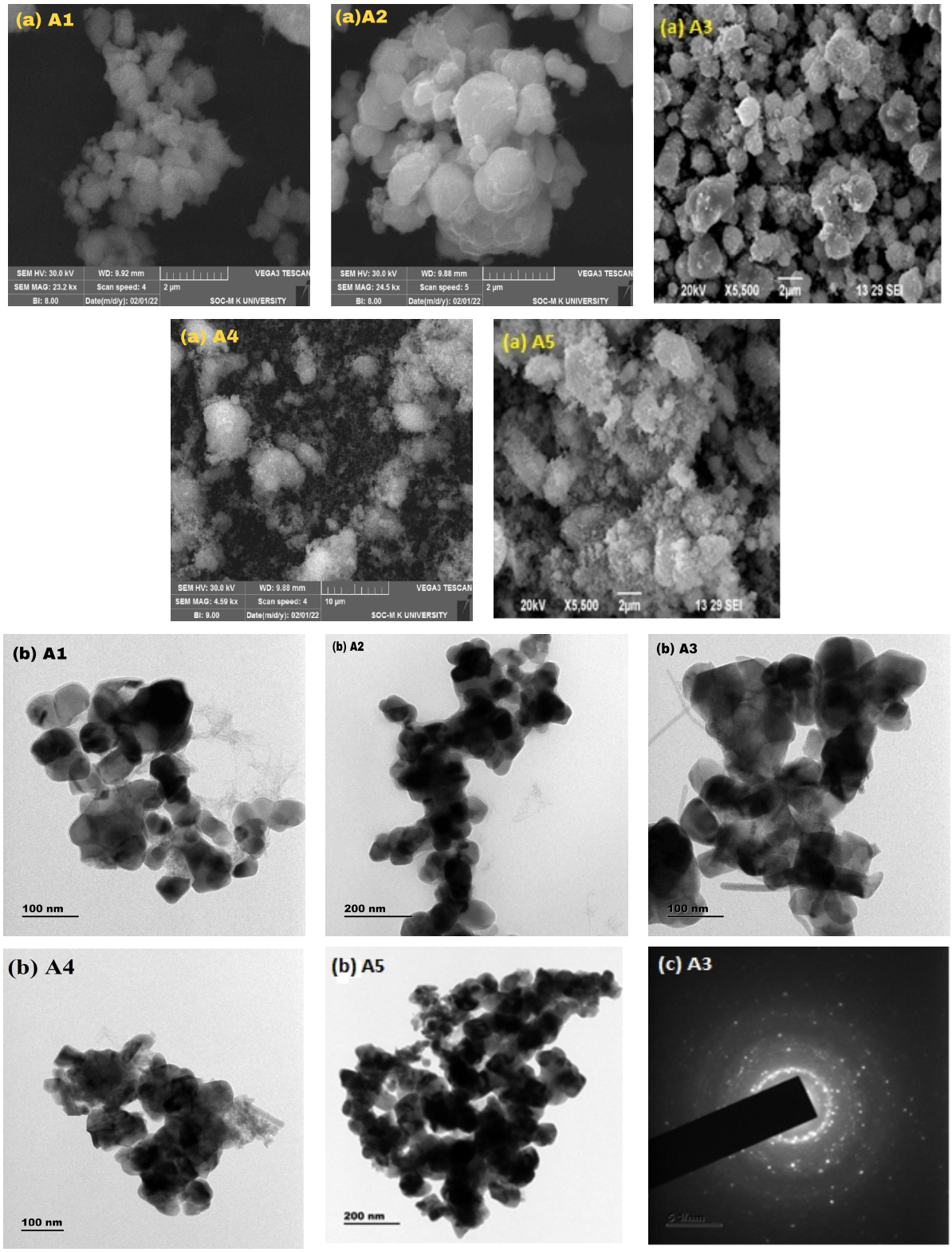

FIG. 2. The SEM images obtained for the $(CdO)_{1-x}(Mn_3O_4)_x$ nanocrystals prepared (a); The TEM images observed for all the five $(CdO)_{1-x}(Mn_3O_4)_x$ nanocrystals, and the SAED pattern for the sample A3 prepared (b,c)

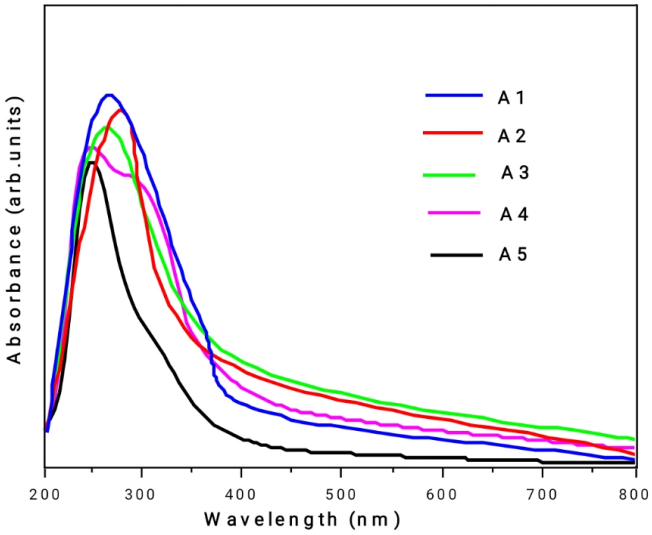

FIG. 3. The UV-visible absorption spectra observed for the (CdO)$_{1-x}$(Mn$_3$O$_4$)$_x$ nanocrystals prepared

crystal grain, crystal grain boundary, ionic, dipolar and electronic contributions to the polarizability [28]. The purity of the nanomaterials under consideration affects the space charge polarization; and the dielectric loss usually takes place due to the absorption of current.

Among the nanocomposites prepared, sample A4 has higher values for the dielectric parameters (ε_r, $\tan\delta$ and σ_{ac}); the D value is minimum for this. The dielectric parameters are found not to vary systematically with the mixed composition (x) in the case of nanocomposites prepared; this results from increased charge carrier and vacancy diffusion along crystal grain boundaries. It is conceivable that the non-synstematic variation of dielectric properties observed as a result of mixing may be caused by non-homogeneity between the crystal grains and crystal grain boundary regions as well as the reduction of movable charges [28].

3.7. Photodegradation of MB dye

The (CdO)$_{1-x}$(Mn$_3$O$_4$)$_x$ samples (A1, A2, A3, A4 and A5) have been investigated with the degradation of Methylene Blue (MB) dye under UV-visible light irradiation and the outcomes obtained are displayed in Fig. 5(a). The photocatalytic activity normally depends on the particle size, optical bandgap energy and particulate surface area of the prepared samples [29]; and this photocatalysis reaction has been used in many medical and environmental applications [30]. In the present study, 100 ml of MB dye solution was added with 50 mg of the prepared sample and stirred for 20 min; the maximum UV-visible light absorption occurred at the wavelength 665 nm and the absorbance decreased as the irradiation time increased (0, 15, 30, 45, 60, 75 and 90 min are the irradiation times used).

The degradation rate was determined by using the pseudo first order kinetic mode,as expressed in Eq. (1) [31]:

$$\log(C_t/C_0) = \log(A_t/A_0) = -k_{\text{app}}t, \tag{1}$$

where C_0 is the intial concentration of MB dye at time 0 (min), k_{app} is the apparent first order rate constant (considered to be the degradation rate in min^{-1} unit), C_t is the final concentration of MB dye at time t (min) and A_0 and A_t are the absorbances at times 0 and t min. The k_{app} values obtained for the samples A1, A2, A3, A4 and A5 are 0.019, 0.152, 0.760, 0.981 and 0.044 min^{-1}, respectively. The k_{app} values observed for the nanocomposites (A2, A3 and A4) are significantly larger than that observed for the end members (A1 and A5); also, for the nanocomposites, the k_{app} value is found to increase with the decrease in x value, which can also be related to the decrease of D value. Karthik *et al.* [2] have found a k_{app} value of 0.0167 min^{-1} for the photocatalytic activity of CdO nanoparticle with MB dye degradation under UV-visible light irradiation; this is in agreement with that found in the present work. Eq. (2) can be used to estimate the degradation percentages:

$$\text{Degradation } (\%) = (A_0 - A_t/A_0) \times 100. \tag{2}$$

The degradation percentages obtained are 62, 85, 88, 95 and 73 %, respectively, for the samples A1, A2, A3, A4 and A5 (with A4 having the maximum degrading efficiency). It has been found that the sample (CdO)$_{0.25}$(Mn$_3$O$_4$)$_{0.75}$ (A4) reacts as a good photocatalyst and better degrades the MB dye under UV-visible light irradiation. Further, Fig. 5(a) shows nearly linear variation of $\log(A_t/A_0)$ with time (t); the recombination of e$^-$/h$^+$ pairs has given easier responses for the degradation [5].

Photocatalytic activity of the un-annealed samples [(CdCO$_3$)$_{1-x}$(Mn$_3$O$_4$)$_x$ nanocomposites, U2, U3 and U4] has also been studied under UV-visible light irradiation for the degradation of MB dye (0, 10, 25, 40, 55 and 70 min are the irradiation times used), and the results obtained are shown in Fig. 5(b). The maximum absorbance of MB dyeis found to

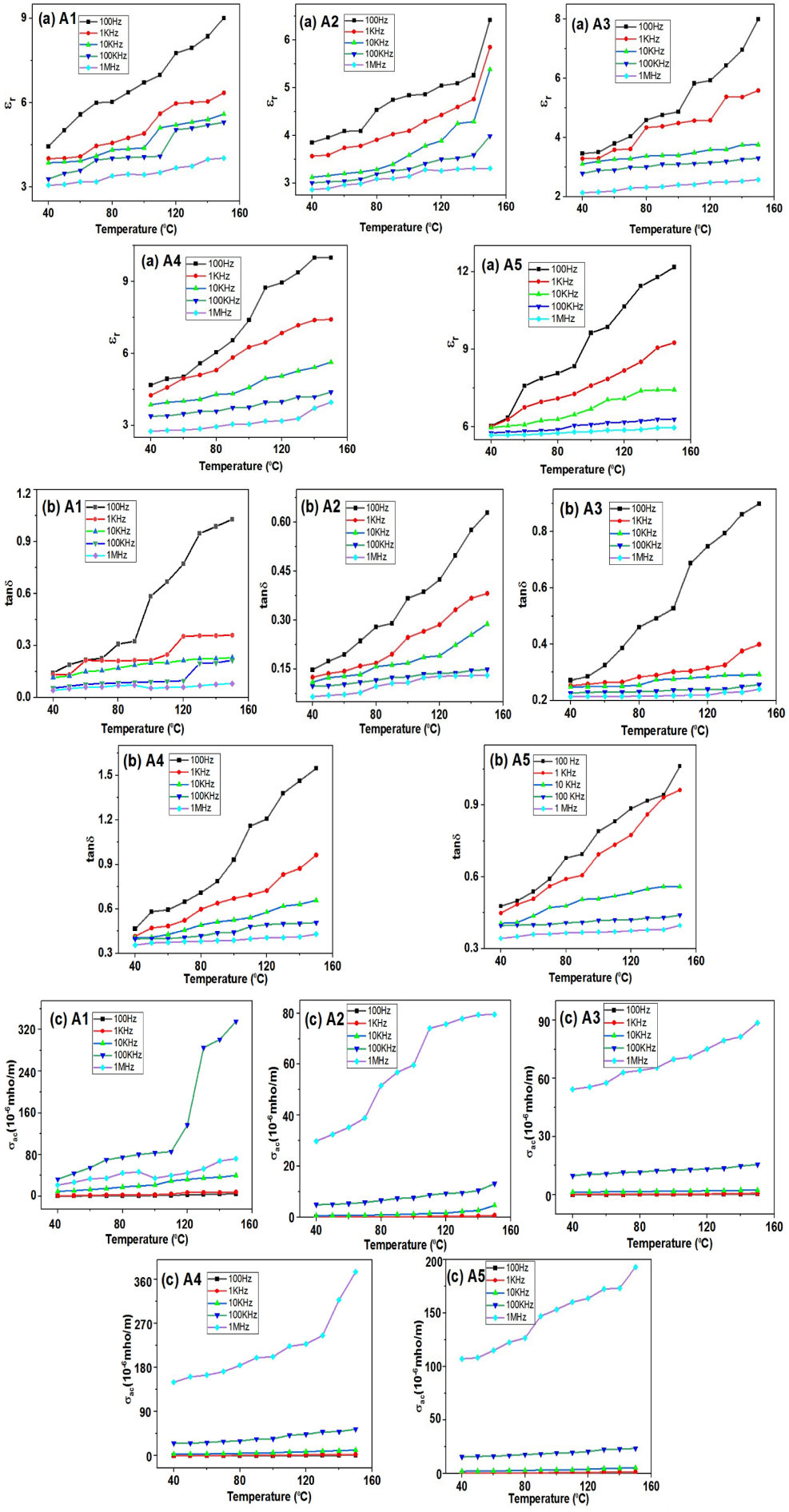

FIG. 4. Temperature dependence of the dielectric constant (ε_r) (a); the dielectric loss factor ($\tan\delta$) (b) and the AC electrical conductivity (σ_{ac}) (c) for the $(CdO)_{1-x}(Mn_3O_4)_x$ nanocrystals prepared

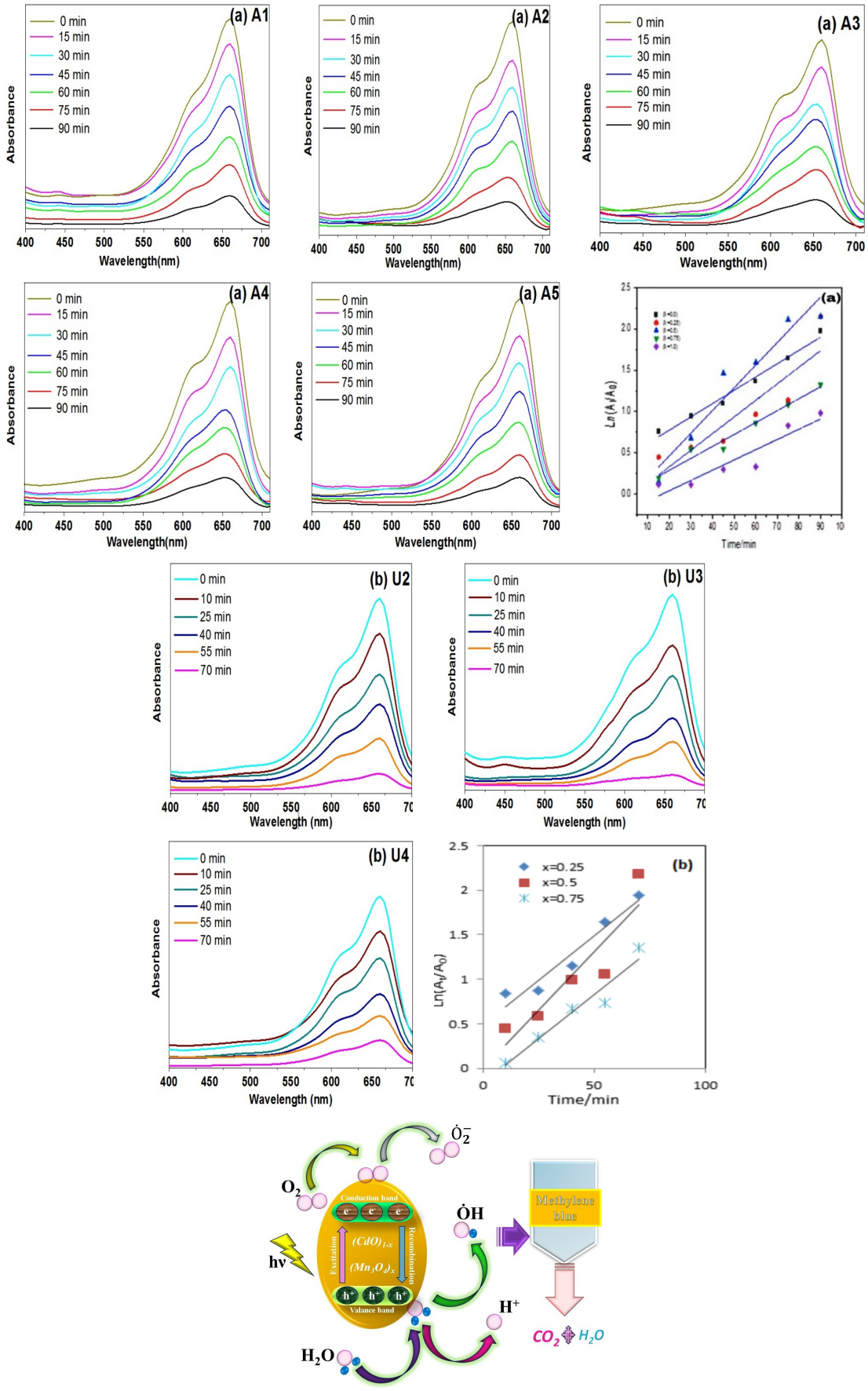

FIG. 5. Photocatalytic degradation curves and the linear plots of $\log(A_t/A_0)$ versus reaction time obtained for the annealed (a) and the un-annealed (b) $(CdO)_{1-x}(Mn_3O_4)_x$ nanocrystals prepared. A schematic diagram of the possible mechanism for the degradation of MB dye over the nanocrystals prepared in the present study (c)

be at 660 nm, and the irradiation time increases with the increasing absorbance. The k_{app} values obtained are 0.011, 0.013 and 0.015, respectively, for the samples U2, U3 and U4; and the photodegradation percentages obtained for the samples U2, U3 and U4 are 44, 49 and 65 % (with U4 having the maximum degrading efficiency), respectively. Fig. 5(b) shows a nearly linear relationship of $\log(A_t/A_0)$ with time (t), which is in line with that observed for the samples A1, A2, A3, A4 and A5.

From the above results, it can be understood that the $(CdO)_{1-x}(Mn_3O_4)_x$ nanocomposites (A2, A3 and A4) exhibit significantly higher photocatalytic activity (photodegradation percentages are in the range of 85 – 95 % in about 90 min) than that exhibited by the $(CdCO_3)_{1-x}(Mn_3O_4)_x$ nanocomposites (U2, U3 and U4) (photodegradation percentages are in the range of 44 – 65 % in about 70 min). The present study indicates that all the three multi-phased $(CdO)_{1-x}(Mn_3O_4)_x$ nanocomposites preapared (A2, A3 and A4) can very well be used to degrade MB dye irradiated with viible light of wavelength around 665 nm for about 90 min. Representation of the band structure and a possible mechanism for the degradation of MB dye over the nanocrystals prepared irradiated with visible light are shown schematically in Fig. 5(c).

On irradiation with light the photogenerated electrons (e^-) are excited from the valence band (VB) to the conduction band (CB) in the photocatalytic oxidation process, while the photogenerated holes (h^+) remain in the valence band. During the process of recombination, the CB electrons and the VB holes can be reduced as shown in Eq. (3).

$$(CdO)_{1-x}(Mn_3O_4)_x + h\nu \rightarrow (CdO)_{1-x}(Mn_3O_4)_x(e^-_{CB} + h^+_{VB}). \tag{3}$$

Consequently, the photogenerated holes of VB can interact with water molecules and produce hydroxyl radicals (OH*). Similarly, the photogenerated electrons of CB can also interact with oxygen to produce superoxide radicals (O_2*^-) as shown in Eqs. (4) and (5).

$$h + + H_2O \rightarrow OH^* + H^+, \tag{4}$$

$$e - + O_2 \rightarrow O_2^{*-}. \tag{5}$$

The hydroxyl and superoxide radicals are considered to be strong oxidation agents [32]. The anions O_2^{*-} do not further contribute to the oxidation process but respond with H^+ for producing HO_2* and e^- for producing OH* radical.

$$O_2^{*-} + H^+ \rightarrow HO_2^*, \tag{6}$$

$$HO_2^* + e^- \rightarrow OH^*, \tag{7}$$

$$\text{MB dye} + (O_2^{*-},\ OH^*) \rightarrow CO_2 + H_2O \text{ (Degradation product)}. \tag{8}$$

Therefore, the electrons and hole (e^-, h^+) pairs have fast recombination for the degradation process. In the present study, the results obtained are found to be highly stable in degradation photocatalytic performance.

3.8. Antimicrobial activity

Investigation on the antimicrobial activities of the annealed samples (A1, A2, A3, A4 and A5) [$(CdO)_{1-x}(Mn_3O_4)_x$ (with $x = 0.0, 0.25, 0.50, 0.75$ and 1.0) nanocrystals] (photographs shown in Fig. 6(a)) and the un-annealed samples (U2, U3 and U4) [$(CdO)_{1-x}(Mn_3O_4)_x$ (with $x = 0.25, 0.50$ and 0.75) nanocrystals] (photographs shown in Fig. 6(b)) have been carried out by the disc diffusion method using Muller Hinton agar against two bacterial pathogens like Gram positive (Bacillus Subtilis, BS), and Gram negative (Escherichia Coli, EC) and the fungus (Candida Albicans, CA). The annealed $(CdO)_{1-x}(Mn_3O_4)_x$ nanocrystals A1, A2, A3, A4 and A5 are marked as RJ1, RJ2, RJ3, RJ4 and RJ5, respectively; the un-annealed $(CdCO_3)_{1-x}(Mn_3O_4)_x$ nanocrystals U2, U3 and U4 are marked as RJ7, RJ8 and RJ9, respectively; The antimicrobial efficiency of nanomaterials commonly depend on the particular surface area, size and morphology [2].

People are exposed to EC from contaminated water and food items, and EC causes urinary infection and traveller's diarrhoea; the BS causes infections such as endocarditis, pneumonia, bacteremia and septicemia. The mechanism of antimicrobial activity involves the nanocrystal prepared as positively charged and the microbe as negatively charged; the thin layer of peptidoglycan is EC, and the thick layer of peptidoglycan is BS [33]. The ROS (Reactive Oxygen Species) penetrates through the cell wall and causes DNA damage and cell death; the great antimicrobial activity of nanomaterials is based on the oxygen species and high oxygen vacancies [34]. Moreover, the antimicrobial activity depends on the zone of inhibition [31].

The zones of inhibition (ZOIs) observed with all the three microbes considered (BS, EC and CA) for the annealed (A1, A2, A3, A4 and A5) and un-annealed (U2, U3 and U4) nanocrystals are shown in Fig. 6(c). Somasundaram *et al.* [5] have reported the antimicrobial activity of CdO with ZOIs observed as 9 and 8 mm, respectively, for the microbes BS and EC. The bacterial activity has been exhibited by the CdO nanocrystal prepared in the present study with ZOIs observed as 22 and 20 mm respectively for BS and EC. For all the eight nanocrystals considered for the study, in general, the ZOIs have been found to be higher with the bacteria (ranging from 16 to 22 mm with BS and 15 to 23 mm with EC) than with the fungus (ranging from 9 to 20 mm with CA); however, the A5 nanocrystal has been found to be more active with all the three microbes considered (18, 23 and 20 mm with BS, EC and CA, respectively). The activities of A3 and A4 have been found to be nearly the same as that of U3 and U4; however, the activity of A2 has been found to be significantly higher than that of U2.

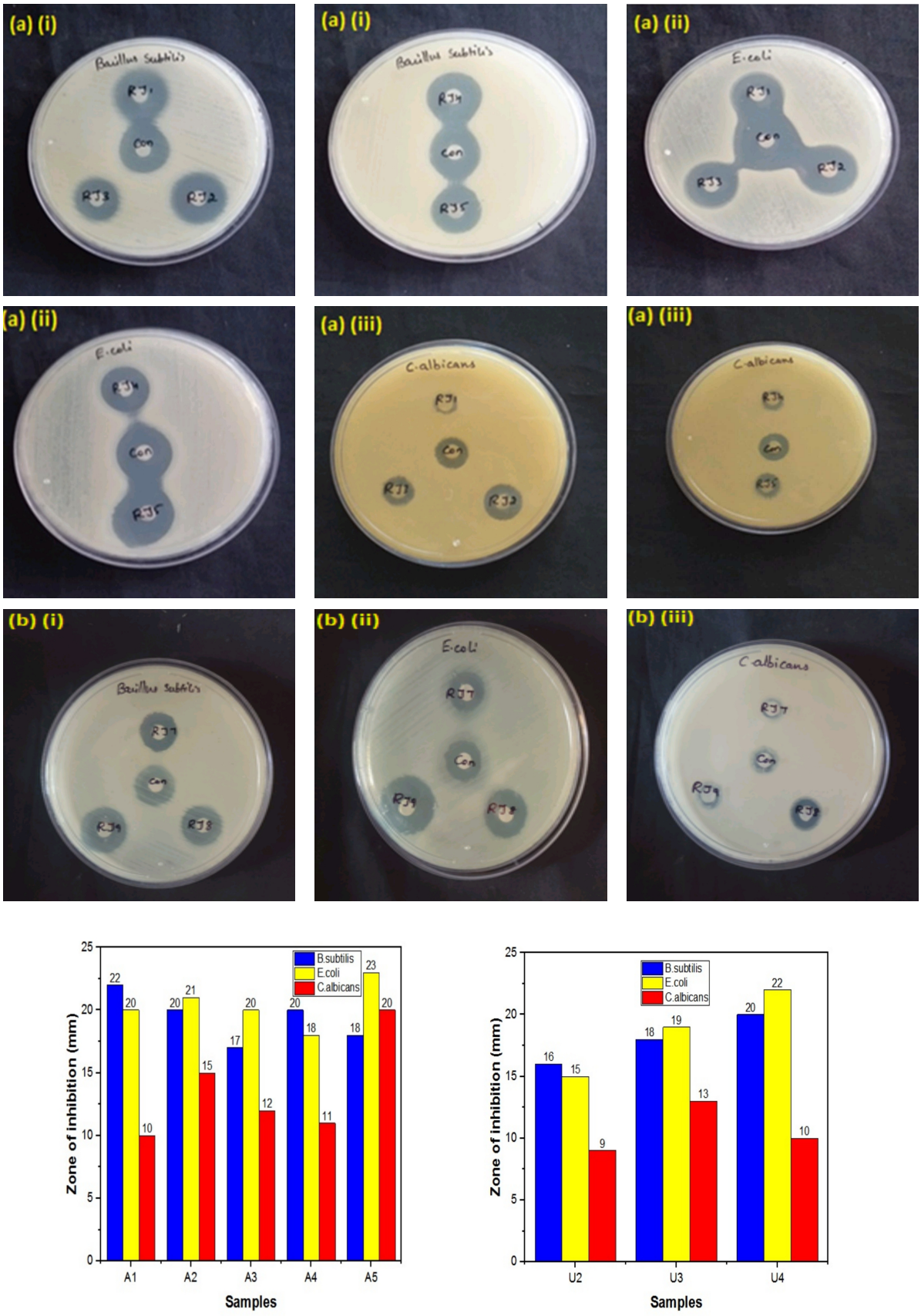

FIG. 6. (a) Observation of ZOIs for the $(CdO)_{1-x}(Mn_3O_4)_x$ nanocrystals (A1, A2, A3, A4 and A5) with: (a)(i) Bacillus Subtilis, (a)(ii) Escherichia Coli and (a)(iii) Candida Albicans. (b) Observation of ZOIs for the $(CdCO_3)_{1-x}(Mn_3O_4)_x$ nanocrystals (U2, U3 and U4) with: (b)(i) Bacillus Subtilis, (b)(ii) Escherichia Coli and (b)(iii) Candida Albicans. (c) Bar graphs showing the ZOIs observed for the $(CdO)_{1-x}(Mn_3O_4)_x$ (A1, A2, A3, A4 and A5) and $(CdCO)_{1-x}(Mn_3O_4)_x$ (U2, U3 and U4) nanocrstals.

4. Conclusion

Nanocrystalline $(CdO)_{1-x}(Mn_3O_4)_x$ (with $x = 0.0, 0.25, 0.50, 0.75$ and 1.0) composites have been successfully prepared by using a simple, fast and low-cost solvothermal technique (using a microwave oven). XRD analysis has revealed phase purity for all the five nanocrystals (A1, A2, A3, A4 and A5) prepared along with revealing the multi-phased composite nature for the three mixed compositions (A2, A3 and A4); the D values obtained are within 38 and 45 nm. EDX spectra have also revealed the high chemical purity and the existence of Cd, Mn and O components in the prepared nanocomposites. SEM and TEM images have indicated nearly spherical morphologies with agglomeration, and SAED pattern shows the polycrystalline nature of the prepared samples. E_g values obtiained from UV-visible spectra are within 4.0 and 5.3 eV; the dielectric measurements at various temperatures and with different frequencies have indicated a normal dielectric behavior for all the five nanocrystals (A1, A2, A3, A4 and A5) studied.

The $(CdO)_{1-x}(Mn_3O_4)_x$ nanocomposites (A2, A3 and A4) have been found to exhibit significantly higher photocatalytic activity than that exhibited by the $(CdCO_3)_{1-x}(Mn_3O_4)_x$ nanocomposites (U2, U3 and U4); results obtained have indicated that the three multi-phased $(CdO)_{1-x}(Mn_3O_4)_x$ nanocomposites preapared can very well be used to degrade MB dye irradiated with light of wavelength around 665 nm. The higher zones of inhibition obtained for all the eight nanocrystals (A1, A2, A3, A4, A5, U2, U3 and U4) studied have indicated a higher antimicrobial activity with the bacteria (BS and EC) than with the fungus (CA); however, the A5 (phase pure Mn_3O_4) nanocrystal has been found to be more active with all the three microbes considered (BS, EC and CA).

References

[1] Yathisa R.O., Arthoba Nayaka Y., Manjunatha P., Vinay M., Purushotham H.T. Effect of doping on the structural, optical and electrical properties of Ni^{2+} doped CdO nanoparticles prepared by microwave combustion route. *Microchemical J.*, 2018, **145** (3), P. 630–641.

[2] Karthik K., Dhanuskodi S., Gobinath C., Prabukumar S., Sivaramakrishnan S. Photocatalytic and antibacterial activities of hydrothermally prepared CdO nanoparticles. *J. Mater. Sci.: Mater. Electron.*, 2017, **28** (15), P. 11420–11429.

[3] Charan Kumar H.C., Rajegowda Shilpa, Sanniaha Ananda. Synthesis of cadmium oxide nanoparticles by electrochemical method: Its photodegradative effects on carboxylic acids and antibacterial behaviours. *J. of Nanoscience and Technology*, 2019, **5** (5), P. 840–845.

[4] Lokanatha Reddy P., Kalim Deshmukh, Chidambaram K., Basheer Ahamed, Kumar Sadasivumi K., Deepalekshmi Ponnamma, Rajasekhar Lakshmipathy, Desagani Dayananda, Khadheer Pasha S.K. Effect of ethylene glycol (PEG) on structural, thermal and photoluminescence properties of CdO nanoparticles for optoelectronics applications. *Materials Today: Proceedings*, 2019, **9**, P. 175–183.

[5] Somasundaram G., Rajan J., Sangaiya P., Dilip R. Hydrothermal synthesis of CdO nanoparticles for photocatalytic and antimicrobial activities. *Results in Materials*, 2019, **4**, 100044.

[6] Christuraj P., Dinesh Raja M., Pari S., Satheesh Kumar G., Uma Shankar V. Synthesis of Mn doped CdO nanoparticles by co-precipitation method for supercapacitor applications. *Materials Today: Proceedings*, 2020, **50** (17), P. 2679–2682.

[7] Krishnaraj S., Anitha R. Photocatalytic degradation analysis of methylene blue aluminium doped cadmium oxide nanoparticles. *J. Advanced Scientic Research*, 2021, **12** (1), P. 75–80.

[8] Munshi A., Prakash T., Ranjith Kumar E., Balamurugan A., Habeebullah T.M., Bawazeer T.M., Abdel-Hafey S.H., El-MetwalyN.M., Indumathi T. Comparative investigation of physicochemical properties of cadmium oxide nanoparticles. *Ceramics International*, 2022, **48** (11), P. 4134–4140.

[9] Xinli Hao, Jinzhe Zhao, Yuehong Song and Zhifang Huang. Synthesis and oxidizability study on Mn_3O_4 nanoparticles. *J. of Nano Research*, 2017, **48**, P. 138–147.

[10] Tanaswini Patra, Jagannath Panda, Tapas Ranjan Sahoo. Synthesis of Mn_3O_4 nanoparticles via microwave combustion route for electrochemical energy storage application. *Materials Today: Proceedings*, 2021, **41**, P. 247–250.

[11] Xiao She, Xinmin Zhang, Jingya Liu, Liang Li, Xianghua Yu, Zhiliang Huang, Songmin Shang. Microwave assisted synthesis of Mn_3O_4 nanoparticles @ reduced graphene oxide nanocomposites for high performance supercapacitors. *Mater. Res. Bulletin*, 2015, **70**, P. 945–950.

[12] Atique Ullah A.K.M., Fazle Kibria A.K.M., Akter M., Khan M.N.I., Tareq A.R.M., Firoz S.H. Oxidative degradation of methylene blue using Mn_3O_4 nanoparticles. *Water Conservation Sci. Eng.*, 2017, **1** (4), P. 249–256.

[13] Rafi Shaik M., Rabbani Syed, Farooq Adil S., Mufsir Kuniyil, Mujeeb Khan, Alqahtani M.S., Shaik J.P., Siddqui M.R.H., Al-Warthan A., Sharaf M.A.F., Abdelgawad, Mahrous Awwad E. Mn_3O_4 nanoparticles: Synthesis, characterization and their antimicrobial and anticancer activity against A549 and MCF-7 cell lines. *Saudi J. Biological Science*, 2021, **28**, P. 1196–1202.

[14] Kalaiselvan C.R., Laha S.S., Somvanshi S.B., Tabish T.A., Thorat N.D., Sahu N.K. Manganese ferrite ($MnFe_2O_4$) nanostructures for cancer theranostics. *Coord. Chem. Reviews*, 2022, **473**, 214809.

[15] Deepa G., Mahadevan C.K. Nanocrystalline composites based on $CdCO_3$ and Mn_3O_4: Synthesis and properties. *J. of Alloys and Compounds*, 2018, **763**, P. 935–950.

[16] Zhen-Yu Yuan, Fan Yang, Hong-Min-Zhu, Fan-Li-Meng, Medhat Ibrahim. High-response n-butanol gas sensor based on ZnO/In_2O_3 heterostructure. *Rare Metals*, 2023, **42** (24), P. 198–209.

[17] Ishfaq M., Hassan W., Sabir M., Somaily H.H., Hachim S.K., Jawad Kadhim Z., Lafta H.A., Alnassar Y.S., Mahdi Rheima A., Rabia Ejaz S., Aadil M. Wet-chemical synthesis of $ZnO/CdO/CeO_2$ heterostructure: A novel material for environmental remediation application. *Ceramics International*, 2022, **48** (23), P. 34590–34601.

[18] Pranesh Shubha J., Shivappa Savitha H., Farooq Adil S., Mujeeb Khan, Rafe Hatshan M., Kavalli K., Shaik B. Straightforward synthesis of $Mn_3O_4/ZnO/Eu_2O_3$-based ternary heterostructure nano-photocatalyst and its application for the photodegradation of methyle orange and methylene blue dyes. *Molecules*, 2021, **26** (15), 4661.

[19] Sundar S.M., Mahadevan C.K., Ramanathan P. On the preparation of ZnO–CdO nanocomposites. *Mater. Manuf. Processes*, 2007, **22** (3), P. 400–403.

[20] Nallendran R., Selvan G., Balu A.R. Photoconductive and photocatalytic properties of CdO–NiO nanocomposites synthesized by a cost effective chemical method. *J. Mater. Sci.: Mater. Electron.*, 2018, **29** (13), P. 11384–11393.

[21] Deepa G., Mahadevan C.K. A facile method to prepare CdO–Mn_3O_4 nanocomposites. *IOSR J. Applied Physics*, 2013, **5** (1), P. 15–18.

[22] Kumar S., Ojha A.K. Synthesis, characterizations and antimicrobial activities of well dispersed ultra-long CdO nanowires. *AIP Advances*, 2013, **3** (5), 052109.

[23] Bousqet-Berthelin C., Stuerga D. Flash microwave synthesis of Mn_3O_4-hausmannite nanoparticles. *J. Mater. Sci.*, 2005, **40** (1), P. 253–255.
[24] Prammitha Rajaram, Ambrose Rejo Jeice, Kumarasamy Jayakumar. Influences of calcination temperature on titanium dioxide nanoparticles synthesized using Averrhoa carambola leaf extract: in vitro antimicrobial activity and UV-lightvcatalyzed degradation of textile wastewater. *Biomass Conversion and Biorefinery*, 2023, **14** (17).
[25] Krasilin A.A., Bodalyov I.S., Malkov A.A., Khrapova E.K., Maslennikova T.P., Malygin A.A. On an adsorption/photocatalytic performance of nanotubular $Mg_3Si_2O_5(OH)_4$/TiO_2 composite. *Nanosystems: Physics, Chemistry, Mathematics*, 2018, **9** (3), P. 410–416.
[26] Kurilenko K.A., Petukhov D.I., Garshev A.V., Shlyakhtin O.A. Anionic redox effect on the electrochemical performance of LLNMC–CeO_2–C nanocomposites. *Nanosystems: Physics, Chemistry, Mathematics*, 2018, **9** (6), P. 775–782.
[27] Nguyen Anh Tien, Chau Hong Diem, Nguyen Thi Truc Linh, Mittova V.O., Do Tra Huong, Mittova I.Ya. Structural and magnetic properties of $YFe_{1-x}Co_xO_3$ ($0.1 \leq x \leq 0.5$) perovskite nanomaterials synthesized by co-precipitation method. *Nanosystems: Physics, Chemistry, Mathematics*, 2018, **9** (3), P. 424–429.
[28] Raja S., Mahadevan C.K. Nanocrystalline solid slabs of pure and CdS added KCl-KBr for energy storage application: Preparation and properties. *Nano-Structures & Nano-Objects*, 2023, **33**, 100938.
[29] Prammitha Rajaram, Yesuvadian Samson, Ambrose Rejo Jeice. Synthesis of $Cd(OH)_2$–CdO nanoparticles using veldt grape leaf extract: Enhanced dye degradation and microbial resistance. *BioNanoScience*, 2023, **13**, P. 1289–1307.
[30] Hosny N.M., Othman E., Dossoki F.I.EI. [Cd(Anthranilate)$_2$]H_2O as a precursor of CdO nanoparticles. *J. of Molecular Structure*, 2019, **1195**, P. 723–732.
[31] Bessy T.C., Bindhu M.R., Johnson J., Shen-Ming Chen, Tse-Wei Chen, Almaary K.S. UV light assisted photocatalytic degradation of textile waste water by $Mg_{0.8-X}Zn_XFe_2O_4$ synthesized by combustion method and in-vitro antimicrobial activities. *Environmetal Research*, 2022, **204** (1), 111917.
[32] Vasiljevic Z.Z., Dojcinovic M.P., Vujancevic J.D., Jankovic-Castvan I., Ognjanovic M., Tadic N.B., Stojadinovic S., Brankovic G.O., Nikolic M.V. Photocatalytic degradation of methylene blue under natural sunlight using iron titanate nanoparticles prepared by modified sol-gel method. *Royal Society Open Science*, 2020, **7** (9), 200708.
[33] Aravind M., Amalanathan M., Sony Michael Mary M. Synthesis of TiO_2 nanoparticles by chemical and green synthesis methods and their multifaceted properties. *SN Applied Sciences*, 2021, **3** (4), 409.
[34] Ancy K., Bindhu M.R., Sunitha Bai J., Gatasheh Mansour K., Atef Hatamleh A., Ilavenil S. Photocatalytic degradation of organic synthetic dyes and textile dyeing waste water by Al and F co-doped TiO_2 nanoparticles. *Environmental Research*, 2022, **206** (12), 112492.

Submitted 6 June 2024; revised 4 September 2024; accepted 8 November 2024

Information about the authors:

Selvaraj Jebisha – Ph.D. Scholar of M.S. University, Tirunelveli, Department of Physics, Annai Velankanni College, Tholayavattam-629167, Tamil Nadu, India; ORCID 0009-0002-0394-697X;

Ganesan Deepa – Departmentof Physics, Pioneer Kumaraswamy College, Nagercoil-629003, Tamil Nadu, India; ORCID 0000-0001-9727-8110; gdeepavinod@ymail.com

Jesumarian Johnson – Department of Physics, Annai Velankanni College, Tholayavattam-629167, Tamil Nadu, India; ORCID 0009-0007-7921-3488;

Chelliah Kamalakshiammal Mahadevan – CSIR Emeritus Scientist, Department of Physics, Bharathidasan University, Tiruchirappalli-620024, Tamil Nadu, India; ORCID 0000-0002-3769-4662; mahadevan58@yahoo.co.in

Conflict of interest: The authors declare that they have no known competing financial interests or personal relationships that could have appeared to influence the work reported in this paper.

Funding: The authors declare that this research did not receive any specific grant from funding agencies in the public, commercial, or not-for-profit sectors.

Author contribution:
S. Jebisha: conceptualization, methodology, investigation, data curation, formal analysis, writing – original draft;
G. Deepa: conceptualization, methodology, validation, supervision, writing – original draft, review and editing;
J. Johnson: methodology, supervision;
C. K. Mahadevan: conceptualization, methodology, validation, writing – original draft, review and editing.